JEE Journal of Ecological Engineering

Volume 19, Issue 1, January 2018, pages 225–232
https://doi.org/10.12911/22998993/79853

Received: 2017.10.10
Accepted: 2017.11.07
Published: 2018.01.01

# Porous Composite for Bipolar Plate in Low Emission Hydrogen Fuel Cells

Renata Wlodarczyk[1]

[1] Department of Energy Engineering, Faculty of Infrastructure and the Environment, Czestochowa University of Technology, Poland, e-mail: rwlodarczyk@is.pcz.czest.pl

**ABSTRACT**

The paper presents the results of graphite-stainless steel composites for the bipolar plates in low-temperature fuel cells. The sinters were performed by powder metallurgy technology. The influence of technological parameters, especially molding pressure were examined. Following the requirements formulated by the DOE concerning the parameters of the materials, it indicated by the value of the parameters. The density, flowability, particle size of graphite and stainless steel powders have been evaluated. Composites have been tested by microstructure and phase analysis, properties of strength, functional properties: wettability, porosity, roughness. The special attention was paid to the analysis of corrosion resistance obtained sinters and influence of technological parameters on the corrosion. Corrosion tests were carried out under conditions simulating the environment of the fuel cell under anode and cathode conditions. The effect of pH solution during working of the cell on corrosion resistance of composites have been evaluated. Contact resistance depends on roughness of sinters. Low ICR determined high contact area GDL-BP and high electrical conductivity on the contact surface. The ICR in anode conditions after corrosion tests are not change significantly; composite materials can be used for materials for BP in terms of $H_2$.

**Keywords:** fuel cells, bipolar plates, graphite composites, structural analysis, corrosion resistance

## INTRODUCTION

Studies on fuel cells today focus on extending their life, limitation of weight and size, and reduction of costs of manufacturing generators. Individual cell is composed of membrane/electrolyte and electrodes at both sides. The whole component is closed at both sides with bipolar or monopolar plates (interconnectors). Bipolar plates (BP) are the key components of generators since they take 80% of weight and 45% of costs of the cell. The mission of the plates is to distribute the fuel and air evenly, conduct electricity between adjacent cells, transfer heat from the cell and prevent from gas leakage and excessive cooling.

According to DOE (the U.S. Department of Energy), basic requirements for materials for bipolar plates in fuel cells include in particular corrosion resistance under fuel cell's operating conditions, low contact resistance, suitable mechanical properties, high thermal and electrical conductivity, low costs of manufacturing. Due to high material and functional requirements, few materials can meet these conditions. Bipolar plates in fuel cells are typically made of non-porous graphite because of its high corrosion resistance. However, low mechanical strength of graphite and high costs connected with processing of graphite elevate the costs of manufacturing of fuel cells. The graphite-based composites modified by steel will allow for obtaining the material with improved mechanical properties, ensuring suitable corrosion resistance and high thermal and electrical conductivity at the same time. The powder metallurgy technology is very useful for obtaining even complicated shape of components, eliminates the problem of mechanical processing of graphite [Wlodarczyk, 2015; Wlodarczyk et al. 2013; Tawfik et al. 2007].

Among the metals used for the construction of BP for low-temperature fuel cells, there are nickel, titanium and a coating made based on these metals [Show et al. 2007]. El-Enim et al.

examined aluminum as layer for BP material [El-Enim et al. 2008]. Nikam et al. suggested copper alloys as materials for BP [Nikam et al. 2006]. The high thermal and electrical conductivity, chemical stability and ease of production make copper very attractive material. On the other hand, a high density copper and its alloys, can disqualify these materials for use in fuel cells.
The most common material in a group of metallic materials is stainless steel [Andre et al. 201; Larijani et al. 2011]. Stainless steel is characterized by high strength, low gas permeability, variety of alloying elements, and above all low production costs. The availability of stainless steels and low cost of production is about their advantages. It is easily shaped into plates with a thickness as low as 0.2 to 1 mm, thus allowing thicknesses still providing channels in the covers mono- or bipolar. The possibility of producing thin plates is associated with a high material density (density of steel approx. 7.80 g $cm^{-3}$), which unfortunately is a disadvantage in these applications. Austenitic steels are usually passivated in the work environment PEM cells [Yang et al. 2011]. The influence of the chemical composition of stainless steel was demonstrated in the works [Husby et al. 2014; Kang et al. 2016].

In the course of research materials complying with the requirements set out by DOE, such requirements proposed sintered stainless steel and composites based on graphite.

The main issue of research was examined the properties of graphite-stainless steel sinters depend on compression pressures. The graphite and stainless steel powders were compressed with 200 MPa, 400 MPa and 700 MPa and sintered in vaccum at 1373K ± 40K for 30 min.

## MATERIALS AND METHODS

In Table 1 depicted selected technological parameters of powders which were used to obtained the sintered composites. The values of technological parameters powders are significantly different from each other (graphite and stainless steel 316L). Twice the value of the powder flow 316LHD indicates the presence of large particles compared to particles of graphite powder, with complicated shapes. Knowledge of fluidity allows you to specify the time required to fill the matrix. They have the greatest flowability of spherical particles, but it is also affected by the particle size of the powder.

Mixtures of graphite powder and 316L stainless steel in amounts of 50 wt.%, filled into the steel matrix and compressed pressure of respectively 200, 400 and 700 MPa. The next step was the sintering of composites in vaccum at 1373K ± 40K for 30 min. The obtained samples were called: G-SS/200, G-SS/400 and G-SS/700, respectively. The height of the samples after pressing and sintering ranged from 3.5 to 4.0 mm. The samples had the shape of disks with a diameter of 50 mm. The size and density of samples meet the general trend of hydrogen technology to reduce size and weight of generators.

Microstructure analysis has been done using scanning electron microscope (SEM) Philips XL30/LaB6 and optical microscope Axiovert. Phase and chemical analysis of composites have been analyzed by XRD (Seifert 3003 T-T) method.

Using the method of mercury porosimetry determined open porosity, bulk density and specific surface area of graphite-stainless steel composites. The mercury porosimeter PoreMaster33 with software Quantachrome Instruments for Window were used. Apparent density takes into account the presence of the connecting channels open pores of the porous material.

In order to determine the surface topography and surface geometry parameters, studies were carried out using a profilometer Hommel T1000 software QuickReport Reader1.2. Tests were performed in triplicate for each sample, the values were averaged. The study of the geometrical structure of materials was carried out using a measuring needle ended with a ball with a radius of 2.5 mm.

In order to determine the type of materials produced under the terms of wettability, applied 3µl water on the surface of the previously polished (paper water, fragmentation 2500) and defatted materials. Wettability test was performed 3–5 times for each sample and the results averaged. The contact angle was determined using a microcamera MicroCapture.

Measurements of ICR between the surfaces of gas diffusion layer (GDL, usually carbon pa-

**Table 1.** Technological parameters of graphite and 316L powders

| Powder | Density [g $cm^{-3}$] | Bulk density [g $cm^{-3}$] | Flowability [s/50 g] |
|---|---|---|---|
| Graphite powder | 2.23 | 0.2 | 13.0 |
| 316LHD powder | 5.60 | 2.67 | 31.0 |

per) and BPs were carried out according to the methodology used by Wang [Wang et al. 2006].

Potentiokinetic tests carried out in 0.1 mol $dm^{-3}$ $Na_2SO_4$ + 2 ppm $F^-$, pH 1.,00, pH 3.00, pH 5.00 at T= 80°C ± 2°C, with scan rate potential 5 mV $s^{-1}$. Potential range changed from cathode potential (-0.8 V vs. SCE- Saturated Calomel Electrode) to anode potential (1.8 V vs. SCE).

## RESULTS AND DISCUSSION

### Structural analysis of graphite-stainless steel composite

Figure 1 shows the microstructure of composite material molded under pressure. Graphite – stainless steel materials have a porous structure with average pore diameter of open reaching up to several tens of micrometers. As follows from the analysis porosimetry, highest among the tested materials involved macropores shows a sample of the G-SS/200.

Analysis of the phase composition of materials of graphite steel showed the presence of the austenite phase (CrFeNi) and graphite hexagonal cell (Fig. 2). Peak centered at approximately 25° comes from $Fe_2O_3$.

### Functional parameters of graphite-stainless steel composite

*Porosity:* The specific pore volume versus pore diameter determined for composite materials was shown in Figure 3. As is apparent from the distribution of pore volume as a function of their diameter, the highest share of macropores, has G-SS/200 sample. The parameter values set for porosimetric measurements are shown in Table 2. The apparent density and open porosity of the composite decreases with increasing compaction pressure materials. The influence of

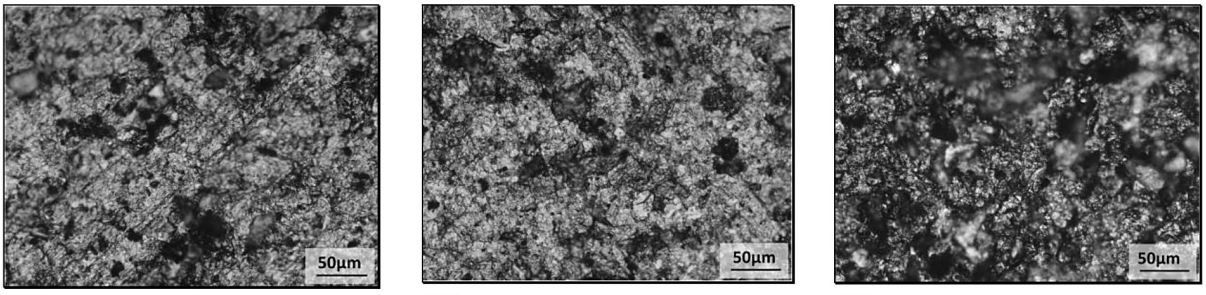


**Fig. 1.** Microstructures of graphite-stainless steel composites – optical microscope; (A) G-SS/200; (B) G-SS/400; (C) G-SS/700

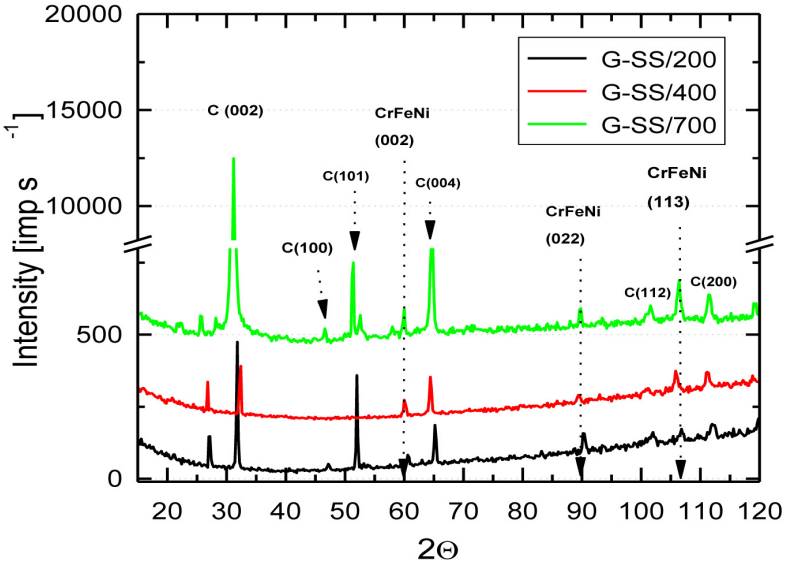


**Fig. 2.** Diffractograms of graphite-stainless steel composites.

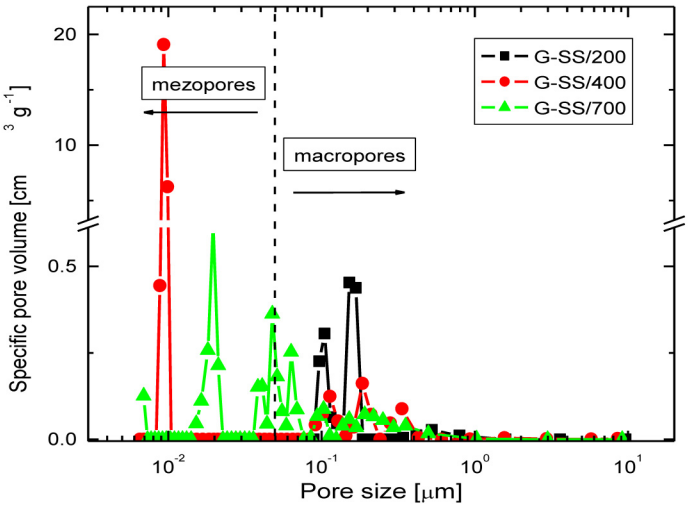


**Fig. 3.** Specific pore volume versus pore diameter determined for composite materials

compaction pressure onto porosity it is observed in Table 5. The lovest porosity is for the material pressed at 700 MPa.

*Wettability:* Materials for bipolar plates are in permanent contact with water: hydrogen and oxygen are humidified before input in fuel cell, the water are produced by the electrochemical process in PEMFC (Proton Exchange Membrane Fuel Cell). The water must be drained effectively in order not to stopped processes. Apart from the suitably shaped channels on the cover and it would be desirable that the material from which the BP have been made not wettable [Ciao et al. 2008]. This is important both from the point of view of cell operation, as well as from the point of view of corrosion of the cell. The water remaining at the surface of the metal leads to initiate corrosive processes. The use of hydrophobic materials, therefore, supports the work of the cell and affect its cost; by implementing hydrophobic materials, auxiliary humidification system of media entering the cell can be simple and uncomplicated [Geng et al. 2010]. To determined the wettability of materials the degree of the contact angle of water drops on the composite surface were estimated. Fig. 4 shows the contact angle Θ (theta) for the tested materials (see Table 2).

**Roughness.** The surface roughness has a significant effect on the corrosion resistance of the materials and the value of the interfacial contact bipolar plate material – diffusion layer (carbon paper). The surface roughness of graphite-steel composite was limited to the value of the parameter Ra of approx. 5.00 μm. Parameters describing the characteristics of the profile are depicted in Table 2.

**Interfacial Contact Resistance.** Figure 5 shows the change in resistance between the surface depending on the compact force. The value of ICR and corrosion resistance significantly influence the work of the cell. Resistance of the material in corrosive conditions can to a certain extent predict the value of the interfacial contact resistance. Hermann at al. [Hermann et al. 2005] demonstrated that stainless steel, titanium, nickel, covered with a layer of oxide in the cell operating conditions, showed high interfacial resistance and high corrosion resistivity because of a passive film on the surface in the acidic environment of the cell. Forming an oxide layer on the metal surface, to some extent it inhibits corrosion processes (provided that the layer is continuous and adheres firmly to the substrate layer thickness in this case is a secondary issue), but it provides an insulating layer which reduces the electrical conductivity [Fu et al. 2009; Pozio et al. 2008]. ICR value depends on the contact area between GDL (Gas

**Table 2.** Parameters of graphite- stainless steel composite with respect to compaction pressure

| Parameters | G-SS/200 | G-SS/400 | G-SS/700 |
|---|---|---|---|
| Density [g cm$^{-3}$] | 2.67 | 2.87 | 2.97 |
| Porosity [%] | 13.68 | 9.74 | 7.42 |
| Specific surface area [m$^2$ g$^{-1}$] | 0.67 | 6.48 | 1.48 |
| Ra [μm] | 5.508 | 4.431 | 4.845 |
| Rz [μm] | 18.84 | 11.33 | 13.43 |
| Contact angle [deg] | 108 | 103 | 91 |
| *ICR* at 140 N cm$^{-2}$ [mΩ cm$^2$] | 33.13 | 42.45 | 47.57 |

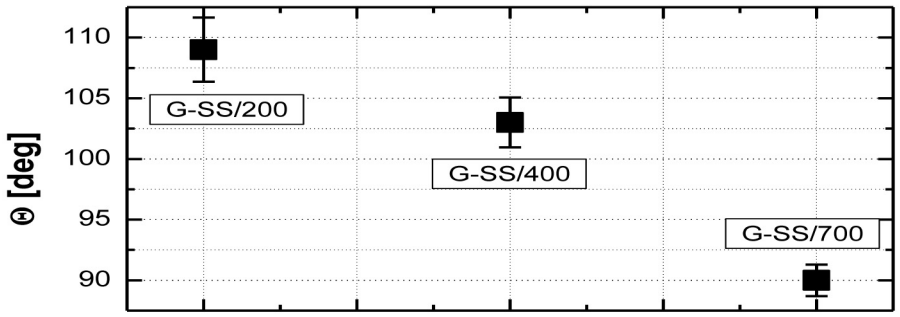


**Fig. 4.** Contact angle evaluated for graphite-stainless steel composites

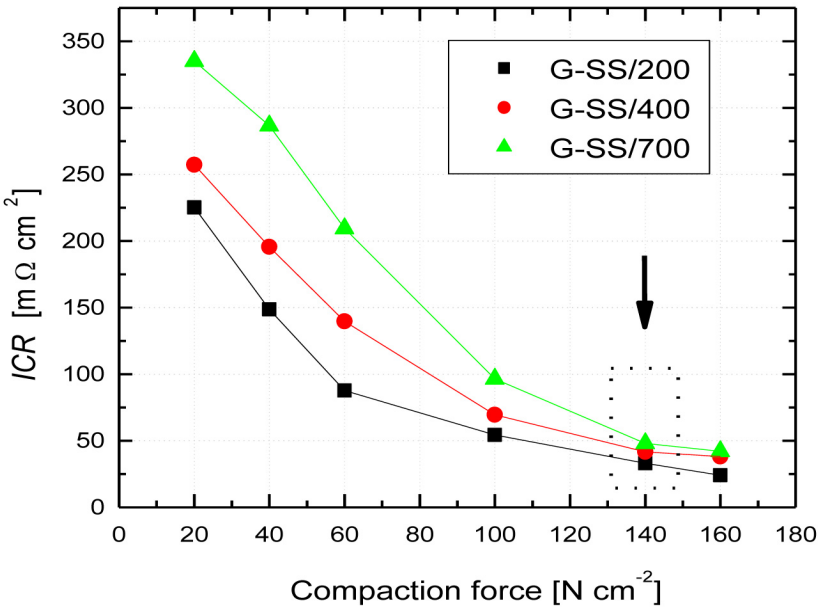


**Fig. 5.** Interfacial contact resistance for composites and carbon paper depending on compaction force

Diffusion Layer) and BP (Bipolar Plates). ICR is a function of pressure per unit of area. Thus, the smoother the surface, the lower should be the ICR. In the case of metal/steel passivated in fuel cells environments, the passive layer make smoother the surface (the passive layer fills the micro- and mesopores) therefore the presence of passive layer should reduced ICR [Tawfik et al. 2007]. Passive layer are formed by metal oxide with a high resistivity. The presence of the passive layer increased the value of ICR. This phenomenon is the result of a high resistivity of passive layers, which inhibits the flow of electrons between the GDL and BP material.

According to data form the literature of the ICR determines contact area or composition, thickness, quality of the passive layer if the material is passivated under operating conditions of the fuel cells [Kraytesberg et al. 2007; Pozio et al. 2008].

The effect of the compaction force on the contact resistance between the composite materials and carbon paper shown in Figure 5. All materials showed a similar pattern: with increasing force, decreasing the value of ICR. This must be attributed to the fact that as the force is increased interfacial contact. Pressing the composites with carbon paper gives an increase in electrical conductivity and thermal conductivity. The characteristic point of the pressure occurring in the stack of fuel cell ratio of 140 N $cm^{-2}$, the composites exhibit comparable, irrespective of the compaction pressure of the composite.

In order to examined the corrosion resistance of materials for bipolar plates in low-temperature fuel cell, different solution can be used for experimental. Corrosion environment could be simulate the conditions in the cell. The pH in the cell changes depending on the stage of the cell operation: in the initial period an acid environment is in the cell,

the acid may be leached out of the membrane used for chemical processing of Nafion® [Fu et al. 2009]. Borup and Vanderborgh [Borup aet al. 1995] suggested that during cell operation, the pH is raised and stabilized at a pH of about 3.60 with fluoride ion concentration of 1.8 ppm at the anode and at pH of 4.02 and a concentration of 1.1 ppm $F^-$ at the cathode. The fluoride ions are derived from the leaching of the membrane (usually Nafion®) during the continued viability of the cell. Other reports in the literature indicate that after reconstruction of the cell operated 500 hours, the concentration of ions at the anode was of the order of magnitude lower [Andre et al. 2010].

As described above, forming the passive layer preferably affect the durability of the material of the cover of the cell, but causes a decrease in the current stack. Within the cell, there is a relative humidity (> 90%), acidity (pH 2.00 – 3.00), high temperature (60–80°C), which may cause the dissolution of the metal [Show at al. 2007]. Losses in potential and current density of fuel cell caused by the presence of passive layer due to the insulating nature of layer (a low conducting metal oxides). As a result of the presence of the passive layer lose its durability also other elements in the cell. Ions and oxides of the passive layer can damage the solid electrolyte and destroy catalyst in MEA. The dissolved metal ions diffuse into the membrane, wherein a block in the exchange of ions within the ionomer, resulting in a lower ionic conductivity, a phenomenon described by Antunes [Antunes et al. 2010]. To minimize the losses caused by the phenomena described, would prepare a film of high electrical conductivity and corrosion resistant with high adhesion at the interface between the layer and substrate. The phenomenon of passivation is to cover the metal with a very thin and resistant coating to protect against corrosion. The main component of the passive layer on the steel is $\gamma$-$Fe_2O_3$. It is also possible to say that the passive layer comprises an inner layer $Fe_3O_4$ and external $\gamma$-$Fe_2O_3$, as during the dissolution of the steel $Fe^{2+}$ produced at lower potentials than ions $Fe^{3+}$. $\gamma$-$Fe_2O_3$ is thermodynamically more stable than $Fe_3O_4$ (which is consistent with the data from the Pourbaix diagram), what provides protective properties of passive layers. The properties of passive layers determines the composition of the steel, environment [46]. With the increase of chromium content in steel increases the thickness of the passive layers.

## The influence of pH solution on corrosion resistance of graphite-stainless steel composites

The graphite used for the bipolar plates of fuel cells, there is passivated with a low-temperature operating conditions of the cell, and therefore does not appear current losses in a stack, due to the reduced permeability of the oxide. The potentiokinetic curves obtained for graphite-stainless steel composites were shown in Figure 6A. The curves are not observed waveform characteristic of a passivating material. In the acidic environment 1.00 pH can be observed a short section in which the change in potential, current values are constant (in potential region 0.73–1.2 V vs. SCE). After crossing the potential 1.2 V vs. SCE can be assumed that the increase in the value of current density is associated with the reconstruction of the passive layer or the formation of pitting under the influence of $F^-$ ions on the surface of the composite. The porous structure of the composite hampered the microscopic analysis of the surface when exposed to corrosive solutions. Analysis of corrosion resistance of composites at pH 3.00 and pH 5.00, did not reveal the tendency of materials to passivate in the test environment.

The effect of pH solution onto potential shows Figure 6B. The value of the recorded potential of the conductive material is the result of processes of reduction of protons (in the solution saturated with $H_2$ – anodic conditions) – (1) or the reduction of $O_2$ (in the case of the saturation solution with $O_2$, cathode conditions) – (2) and the oxidation of the metal (3):

$$4H^+ + 4e^- \rightarrow 2H_2 \quad (1)$$

$$O_2 + 4H^+ + 4e^- \rightarrow 2H_2O \quad (2)$$

$$Me \rightarrow Me^{n+} + ne^- \quad (3)$$

Water is produced in oxygen reduction reaction, Me describes all the metals contained in the material that oxidize $Me^{n+}$ ions go into solution and to provide a suitable amount of electrons $ne^-$. When measuring potential at open, not saturated with a solution of any of these gases to determine the effects of solution pH. In pH 1.00 solution the circuit open potential value of the composite decreased from 0.28V vs. SCE to -0.38V vs. SCE and then stabilized at this level after ca. 400 sec. In solution with higher pH G-SS/400 sample, the initial value potential is

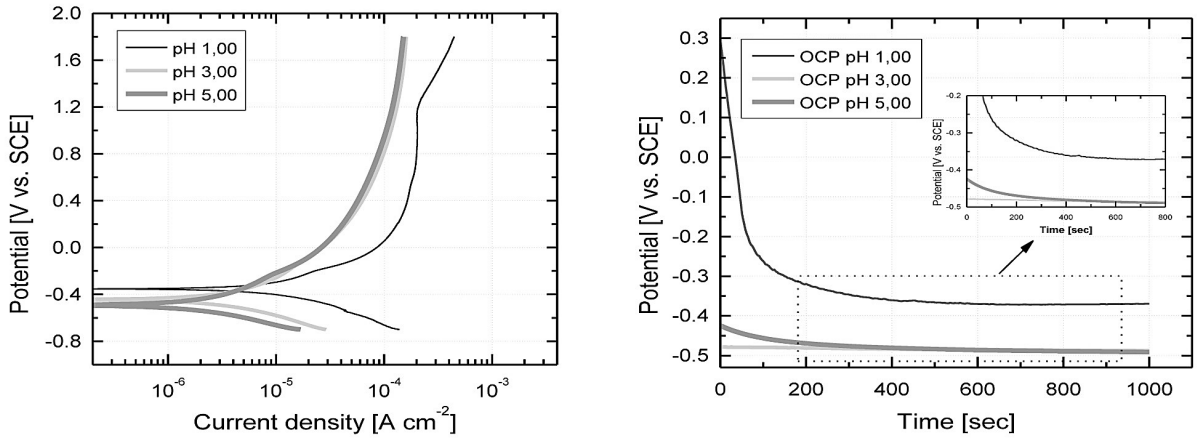


(A) (B)

**Fig. 6.** (A) Potentiokinetic curves obtained in solution with different pH for G-SS/400, (B) open circuit potential obtained for G-SS/400

**Table 3.** Corrosion parameters estimated from potentiokinetis curves show in Figure 6

| | Materials | $E_{corr}$ [V vs. SCE] | $i_{corr}$ [A cm$^{-2}$] | *Rp* [kΩ cm$^2$] | *i* at -0.1V vs. SCE [A cm$^{-2}$] | *i* at 0.6V vs. SCE [A cm$^{-2}$] |
|---|---|---|---|---|---|---|
| pH 1.00 | G-SS/200 | -0.382 | $8.15 \cdot 10^{-6}$ | 34 | $4.44 \cdot 10^{-5}$ | $1.32 \cdot 10^{-4}$ |
| | G-SS/400 | -0.377 | $7.79 \cdot 10^{-6}$ | 39 | $3.37 \cdot 10^{-5}$ | $1.75 \cdot 10^{-4}$ |
| | G-SS/700 | -0.369 | $4.10 \cdot 10^{-6}$ | 51 | $3.45 \cdot 10^{-5}$ | $1.47 \cdot 10^{-4}$ |
| pH 3.00 | G-SS/200 | -0.376 | $6.53 \cdot 10^{-6}$ | 156 | $1.78 \cdot 10^{-5}$ | $6.23 \cdot 10^{-4}$ |
| | G-SS/400 | -0.399 | $3.61 \cdot 10^{-6}$ | 163 | $1.53 \cdot 10^{-5}$ | $6.85 \cdot 10^{-5}$ |
| | G-SS/700 | -0.319 | $3.47 \cdot 10^{-6}$ | 165 | $1.57 \cdot 10^{-5}$ | $6.97 \cdot 10^{-5}$ |
| pH 5.00 | G-SS/200 | -0.483 | $2.45 \cdot 10^{-6}$ | 218 | $1.50 \cdot 10^{-5}$ | $6.83 \cdot 10^{-4}$ |
| | G-SS/400 | -0.473 | $2.27 \cdot 10^{-6}$ | 206 | $1.46 \cdot 10^{-5}$ | $6.56 \cdot 10^{-5}$ |
| | G-SS/700 | -0.456 | $2.55 \cdot 10^{-6}$ | 242 | $1.50 \cdot 10^{-5}$ | $6.39 \cdot 10^{-5}$ |

observed at -0.42V vs. SCE in pH 3.00 and -0.48 V vs. SCE in pH 5.00 solutions. In both pH (3.00 and 5.00) the potential value was stabilized at -0.50 V vs. SCE. The higher open circuit potential conditions, the slower processes of corrosion (corrosion is delayed).

Analyzing the corrosion parameters estimated on the basis of registered potency kinetic curves, the corrosion current density fulfills the requirements set out by the DOE [Show et al. 2007]. Polarization resistance as a parameter corrosion resistance indicates that the highest stability in the operating conditions of the fuel cell of the tested composites exhibits G-SS/700, regardless of pH. The value of current density in anode conditions (E= -0.1V vs. SCE) and cathode conditions (E= 0.6V vs. SCE) are almost comparable to the materials: $10^{-5}$ A cm$^{-2}$ near anode and $10^{-4}$ A cm$^{-2}$ near cathode (see Table 3). The potentiokinetic curves obtained for G-SS/200 and G-SS/700 did not put in paper. The value of current density not meet the requirements of DOE.

## CONCLUSIONS

Currently, one of the priority tasks is to ensure that future generations of energy sources and replacement of energy systems from fossil fuels in favor of renewable sources and hydrogen. Using hydrogen as an energy carrier, it is necessary to use a generator to enable its combustion or a device called a fuel cell.

Construction and operation of the fuel cell are clearly defined and well understood. Properly selected material on the element ensures proper operation of the cell with high efficiency and extending component life. As part of this work is designed and tested characteristics of materials intended for the construction of bipolar plates low-temperature fuel cells.

The performed analysis of the properties of graphite – 316L composites allows to formulate the following statements:

- powder metallurgy technology allows to obtain a product with the desired properties by selection of process parameters such as the

composition of the mixed powders and pressing pressure
- irrespective of the composition of the composite and the molding pressure produced materials belong to the group of hydrophobic materials.
- the apparent density of the sinter is proportional to the compaction pressure and the value thereof is inversely proportional to the compaction pressure;
- change the geometry of the surface is clearly visible in the form of high-value ICR, due to the limited number of contact points on the border of the cover-carbon paper;
- composites with a 50 wt. % addition does not passivate the steel, and the corrosion current density values indicate a high resistance material in an anode and cathode of the fuel cell;
- the ICR in anode conditions after corrosion tests are not change significantly; composite materials can be used for materials for BP in terms of $H_{2.}$

## REFERENCES


1. Andre J, Antoni L, Petit J-P, 2010. Corrosion resistance of stainless steel bipolar plates in a PEMFC environment: A comprehensive study. Int J Hydrogen Energy; 35: 3684–97.
2. Antunes RA, Oliveira MCL, Ett G, Ett V, 2010. Corrosion of metal bipolar plates for PEM fuel cells: A review. Int. Journal of Hydrogen Energy; 35: 3632–47.
3. Borup RL, Vanderborgh NE, 1995. Design and testing criteria for bipolar plate materials for PEM fuel cell applications. Mater Res Soc Symp Proc; 393: 151–5.
4. Ciao K, Zhou B, 2008. Effects of electrode wettabilities on liquid water behaviors in PEM fuel cell cathode. J. Power Sources; 175: 106–19.
5. El-Enim SAA, Abdel-Salam OE, El-Abd H, Amin AM, 2008. New electroplated aluminum bipolar plate for PEM fuel cell. J Power Sources; 177: 131–136.
6. Fu,Y, Lin G, Hou M, Wu B, Li H, Hao L, Shao Z, Yi B, 2009. Optimized Cr-nitride film on 316L stainless steel as proton exchange membrane fuel cell bipolar plate, Int J Hydrogen Energy; 34: 453–58.
7. Geng S, Li Y, Ma Z, Wang L, Wang F., 2010. Evaluation of electrodeposited Fe-Ni Alloy on ferritic stainless steel solid oxide fuel Cell. J Power Sources; 195: 3256–60.
8. Hermann A, Chaudhuri T, Spagnol T, 2005. Bipolar plates for PEM fuel cells: A review. Int. J. Hydrogen Energy; 30: 1297–302.
9. Husby H, Kongstein OE, Oedegaard A, Seland F, 2014. Carbon-polymer composites coatings for PEM fuel cell bipolar plates, Int J Hydrogen Energy; 39: 951–57.
10. Kang K, Park S, Jo A, Lee K, Ju H, 2016. Development of ultralight and thin bipolar plates using epoxy-carbon fiber prepregs and graphite composites. Int. Journal of Hydrogen Energy; http://dx.doi.org/10.1016/jijhydene (2016.05.27).
11. Kraytsberg A, Auinat M, Ein-Eli Y, 2007. Reduced contact resistance of PEM fuel cell's bipolar plates via surface texturing. J Powers Sources; 164: 697–703.
12. Larijani MM, Yari M, Afshar A, Jafarian M, Eshghabadi M, 2011. A comparison of carbon coated and uncoted 316L stainless steel for using as bipolar plates in PEMFCs. J Alloys and Comp;509: 7400–04.
13. Nikam VV, 2006. Reddy RG, Copper alloy bipolar plates for polymer electrolyte membrane fuel cell. Electrochim Acta; 51: 6338–45.
14. Nikam VV, Reddy RG, 2005. Corrosion studies of a copper-berylium alloy in a simulated polymer electrolyte membrane fuel cell environment. J Power Sources; 152: 146–55.
15. Pozio A, Silva RF, Masci A, 2008. Corrosion study of SS430/Nb as bipolar plate materials for PEMFCs. Int J Hydrogen Energy; 33: 5697–702.
16. Shimpalee S., Lilavivat V, McCrabb H, Khunatorn Y, Lee H-K, Lee W-K, Weidner JW, 2016. Investigation of bipolar plate materials for proton exchange membrane fuel cells. Int. Journal of Hydrogen Energy; http://dx.doi.org/10.1016/jijhydene (2016.05.16).
17. Show Y, 2007. Electrically conductive amorphous carbon coating on metal bipolar plates for PEFC. Surf Coat Technol; 202: 1252–5.
18. Show Y, Miki M, Nakamura T, 2007. Increased in output power from fuel cell used metal bipolar plate coated with a – C film. Diamond Relat Mater; 16: 1159–61.
19. Tawfik H, Hung Y, Mahajan D, 2007. Metal bipolar plates for PEM fuel cell – A review. J. Power Sources; 163: 755–63.
20. Wang SH, Peng J, Lui WB, Zhang JS, 2006. Performance of the gold-plated titanium bipolar plates for the light weight PEM fuel cells. J Power Sources; 162: 486–91.
21. Wlodarczyk R, 2015. Porous carbon materials for elements in low-temperature fuel cells. Arch Metall Mater; 60(1): 117–20.
22. Wlodarczyk R, Wrońska A, 2013. Effect of pH on corrosion of sintered stainless steels used for bipolar plates in polymer exchange membrane fuel cells. Arch Metall Mater; 58(1): 89–93.